LAWRENCE
LIVERMORE
NATIONAL
LABORATORY

LLNL-JRNL-516911

HYBRID-LIKE 2/1 FLUX-PUMPING ANDMAGNETIC ISLAND EVOLUTION DUE TO EDGE LOCALIZED MODE-TEARING MODE COUPLING IN DIII-D

J. D. King, R. J. LaHaye, C. C. Petty, T. H. Osborne, C. J. Lasnier, R. J. Groebner, F. A. Volpe, M. J. Lanctot, M. A. Makowski, C. T. Holcomb, W. M. Solomon, S. L. Allen, T. C. Luce, M. E. Austin, W. H. Meyer, E. C. Morse

November 29, 2011

Physics of Plasmas

Disclaimer

GA–A27069

HYBRID-LIKE 2/1 FLUX-PUMPING AND MAGNETIC ISLAND EVOLUTION DUE TO EDGE LOCALIZED MODE-TEARING MODE COUPLING IN DIII-D

by
J.D. KING, R.J. La HAYE, C.C. PETTY, T.H. OSBORNE,
C.J. LASNIER, R.J. GROEBNER, F.A.G. VOLPE, M.J. LANCTOT,
M.A. MAKOWSKI, C.T. HOLCOMB, W.M. SOLOMON, S.L. ALLEN,
T.C. LUCE, M.E. AUSTIN, W.H. MEYER and E.C. MORSE

SEPTEMBER 2011

GENERAL ATOMICS

DISCLAIMER

GA–A27069

HYBRID-LIKE 2/1 FLUX-PUMPING AND MAGNETIC ISLAND EVOLUTION DUE TO EDGE LOCALIZED MODE-TEARING MODE COUPLING IN DIII-D

by
J.D. KING,[1,2] R.J. La HAYE, C.C. PETTY, T.H. OSBORNE, C.J. LASNIER,[1] R.J. GROEBNER, F.A.G. VOLPE,[3] M.J. LANCTOT,[1] M.A. MAKOWSKI,[1] C.T. HOLCOMB,[1] W.M. SOLOMON,[4] S.L. ALLEN,[1] T.C. LUCE, M.E. AUSTIN,[5] W.H. MEYER[1] and E.C. MORSE[2]

This is a preprint of a paper to be submitted for publication in Physics of Plasmas.

[1]Lawrence Livermore National Laboratory, Livermore, California
[2]University of California, Berkeley, California
[3]University of Wisconsin, Madison, Texas
[4]Princeton Plasma Physics Laboratory, Princeton, New Jersey
[5]University of Texas, Austin, Texas

Work supported by
the U.S. Department of Energy
under DE-AC52-07NA27344, DE-FG03-89ER51116,
DE-FC02-04ER54698, DE-FG02-92ER54139
and DE-FG03-97ER54415

GENERAL ATOMICS ATOMICS PROJECT 30200
SEPTEMBER 2011

ABSTRACT

Direct analysis of internal magnetic field pitch angles measured using the motional Stark effect diagnostic shows $m/n = 2/1$ neoclassical tearing modes exhibit stronger poloidal magnetic flux-pumping than typical hybrids containing $m/n = 3/2$ modes. This flux-pumping causes the avoidance of sawteeth, and is present during partial electron cyclotron current drive suppression of the tearing mode. This finding could lead to hybrid discharges with higher normalized fusion performance at lower q_{95}. The degree of edge localized mode-neoclassical tearing mode (ELM-NTM) coupling and the strength of flux-pumping increase with beta and the proximity of the modes to the ELMing pedestal. Flux-pumping appears independent of magnetic island width. Individual ELM-NTM coupling events show a rapid timescale drop in the island width followed by a resistive recovery that is successfully modeled using the modified Rutherford equation. The fast transient drop in island width increases with ELM size.

I. INTRODUCTION

High performance advanced inductive hybrid discharges have been realized in ASDEX-U [1], JET [2], JT-60U [3], and DIII-D [4] tokamaks. The goal of the hybrid scenario is to extend the length of ITER standard H-mode pulses by reducing the inductive current requirement [5]. These discharges contain ~50% non-inductively driven plasma current and exhibit good energy confinement. In almost all cases a neoclassical tearing mode (NTM) is present throughout the stationary phase of the discharge where average plasma conditions are constant for times longer than the current profile relaxation time. In the DIII-D tokamak [6], stationary hybrids with $3 < q_{95} < 4.5$ achieve normalized fusion performance [5] ($G \equiv \beta_N H_{89P} / q_{95}^2$) in excess of that required for $Q_{fus} = 10$ operation in ITER [5]. Here Q_{fus} is the fusion gain defined by the ratio of fusion output power to injected power and is proportional to G, the normalized fusion performance. The plasma pressure is described by normalized beta $\beta_N \equiv \beta/(I/aB)$, where β is the kinetic plasma pressure over the magnetic pressure, I is the total plasma current, a is minor radius, and B is toroidal field. H_{89P} is the dimensionless enhancement factor of the energy confinement based on the ITER 1989 L-mode scaling [7]. The safety factor at the 95% normalized poloidal flux surface is written as q_{95}.

Although counter-intuitive, thus far the greatest hybrid performance has been found in discharges with core MHD instabilities present. In DIII-D $q_{95} \sim 3$ discharges (highest G), both sawteeth and $m/n = 3/2$ tearing instabilities are present, while for $q_{95} > 4$ (lower G) only a 3/2 NTM exists (m is the poloidal mode number and n is the toroidal mode number). Recent advanced inductive low torque experiments, with similar discharge parameters as are expected in ITER hybrids, have shown a propensity to develop only 2/1 NTMs at lower onset beta [8] instead of 3/2 modes.

The avoidance of sawteeth in higher q_{95} cases is tied to the presence of a 3/2 NTM [9], which couples to edge localized modes (ELM) and causes repeated rapid relaxations of the current profile [10]. With each edge localized mode-neoclassical tearing mode (ELM-NTM) coupling event, poloidal flux is pumped from the core to the edge of the plasma across the 3/2 rational surface. Throughout this work the transport of poloidal flux across the rational surface of an NTM is referred as "flux-pumping" [10]. Note that no internal flux measurement is made. Instead changes in flux are inferred from measurements of the vertical magnetic field strength. By flattening the toroidal plasma current profile, q outside the 3/2 rational surface decreases and q inside the rational surface increases. For the normally rapid ELMs on DIII-D, the minimum safety factor ($q_{\min}$) stays above unity and the $m/n = 1/1$ sawtooth is not destabilized. This magnetic flux-pumping is measured directly from motional Stark effect (MSE) polarimeter [11,12] data using Ampere's law [13] without equilibrium reconstruction. Later in this work we will show that magnetic flux-pumping is not unique to the 3/2 NTM.

In the higher performing hybrid discharges (q_{95} ~3) normalized beta is limited to a value ~20% smaller than the no-wall limit [5] ($\beta_N \sim 4l_i$), where l_i is the plasma internal inductance. This is partly due to the sawteeth triggering 2/1 NTMs. Advanced inductive hybrid discharges have mostly focused on increasing plasma performance without active stability or current profile control. From the findings presented in this work, it appears that the partial suppression of a 2/1 mode may have a double benefit of allowing higher achievable β_N while providing intrinsic sawtooth avoidance in lower q_{95} discharges. Furthermore, much progress has been made in efficient electron cyclotron current drive (ECCD) NTM stabilization [14–16]; routine use of this technique is expected in future devices.

The rest of this paper is organized as follows. In Sec. II a stationary hybrid-like sawtooth free discharge is presented containing a 2/1 NTM that exhibits flux-pumping. Section III shows 2/1 flux-pumping during a period of partial ECCD suppression [17] and discusses how a few parameters influence the strength of the flux-pumping. The physics of ELM-NTM coupling is discussed in Sec. IV. Also, a clear connection between ELM size and the strength of the individual coupling events is presented. Section V provides some concluding remarks.

II. 2/1 STATIONARY HYBRID DISCHARGE

Figure 1 shows a successful hybrid discharge (red) and a similar discharge where a saturated 2/1 NTM was generated instead of a 3/2 mode (black). It can be seen in the black case that β_N drops by ~13%, while beta feedback control causes the neutral beam power to increase from 5 to 9 MW in an attempt to sustain the target beta. This degradation in confinement is significant enough that the discharge would not be considered a high performance hybrid. However, the two cases have similar safety factor profiles, with $q_{95} \sim 4.4$, and $q_{\min}$ being maintained above unity. Accordingly, no sawteeth are observed in either case evidenced by the absence of periodic drops in the core soft x-ray diagnostic signals. Both plasmas have comparable resistance R_p and therefore similar current relaxation times (τ_R). The discharge containing the 2/1 can be considered "hybrid-like" in that stationary plasma parameters are maintained for times longer than τ_R after the NTM saturates.

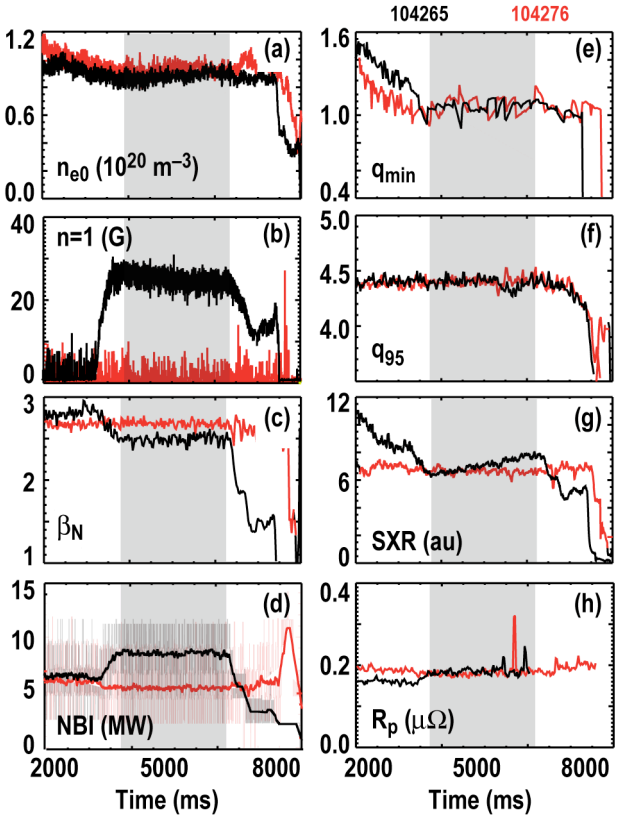

Fig. 1. Black – a hybrid-like discharge containing a 2/1 NTM. Red – a typical hybrid discharge containing only a 3/2 NTM (a) Central electron density (10^{20} m^{-3}) (b) Mirnov probe amplitude of n=1 mode (G) (c) normalized beta (d) total (light) and averaged (dark) injected neutral beam power (MW) (e) minimum safety factor (f) edge safety factor (g) core soft x-ray signal (arb. units) (h) average plasma resistivity ($\mu\Omega$).

During the stationary period of the discharge an average measured MSE pitch angle for each channel is determined 5 ms before, and 5 ms after a series of ELM events. The internal current profile before and after the ensemble average of ELM events is then calculated directly from Ampere's law [12], rather than from an equilibria reconstruction, allowing the average change in the q-profile across the ELM event to be determined.

The periodic change in the q-profile, characteristic of 3/2-hybrid discharges, is also seen in hybrids that develop 2/1 NTMs. Figure 2 shows the change in the q-profile for a poor confinement hybrid-like plasma containing a saturated 2/1 NTM. This change in safety factor is consistent with a shift in the externally driven current density from inside to outside the $q = 2$ surface. The largest increase in the q value inside the 2/1 rational surface is just under 0.06, which is more than twice that measured in a previous work [10] for a 3/2-hybrid at similar q_{95} and normalized beta. Also, the change in q shows a zero crossing occurring at the 2/1 rational surface.

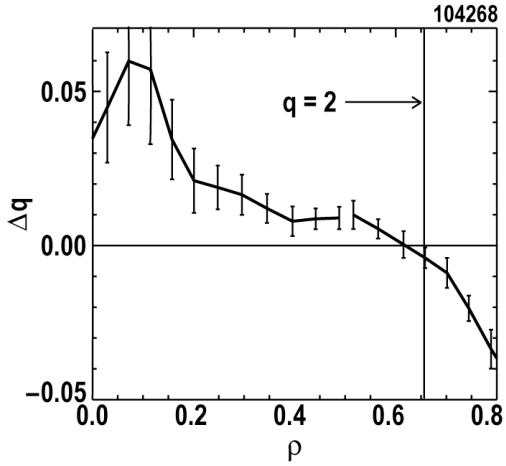

Fig. 2. Change in the safety factor profile measured through direct MSE analysis using Ampere's law and ensemble averaged over 44 ELM events. ρ is the normalized minor radius.

This stronger 2/1 flux-pumping should mean that 2/1-hybrids can operate without sawteeth at lower q_{95}, or with less frequent ELMing. A lower q_{95} discharge with $q_{\min} > 1$ requires a broader safety factor profile than higher q_{95} cases. Stronger flux-pumping results in greater flattening of the safety factor profile per ELM event. Recall, lower q_{95} discharges contain smaller relaxed values of $q_{\min}$. For higher q_{95} discharges less frequent ELMs are required since each ELM event produces a greater change in $q_{\min}$.

Later, it is shown that the strength of the ELM-2/1 tearing mode coupling is related to the radial proximity of the ELM to the NTM. This agrees with the finding of stronger flux-pumping in the 2/1 case since the 2/1 NTM is located closer to the ELMing pedestal than the 3/2 mode.

III. EFFECT OF SUPPRESSION

Stronger 2/1 flux-pumping may enable sawtooth free hybrid operation at lower q_{95} and higher β_N for the same ELM frequency, compared to conventional 3/2-hybrids. However, achieving higher normalized fusion performance will require a significant improvement in energy confinement in the presence of the 2/1 mode. Complete suppression [18] and prevention [19] of the 2/1 NTM using ECCD has shown that $\beta_N \sim 4l_i$ can be achieved in hybrid discharges. From this work, it appears that a hybrid containing a partially suppressed 2/1 NTM could mitigate most of the loss in confinement due to the mode while producing a flatter average current profile from inherent plasma flux-pumping. In this section, requirements for a partially suppressed 2/1-hybrid are outlined and the effect of active suppression on flux-pumping is shown.

As was seen in the previous section, confinement degradation of a 2/1 NTM is greater than that of an equivalent 3/2 island, as a consequence of the larger minor radius of the 2/1 rational surface. This can be illustrated by considering the magnetic island belt model [19], where for a cylindrical plasma the confinement time degradation is described as,

$$\frac{\tau_{inc}}{\tau_{inc0}} = 1 - \frac{4 r_s^3 w}{a^4} \quad , \tag{1}$$

where τ_{inc} and τ_{inc0} are the incremental energy confinement time with and without a tearing mode respectively, r_s is the minor radius of the rational surface, w is the full magnetic island width, and a is the total plasma minor radius. Note the cubic variation with the rational surface minor radius.

Successful sawtooth free stationary hybrid discharges in DIII D have been found to contain a 3/2 NTM ~6 to 8 cm wide [20]. Considering a single 3/2-hybrid q-profile, for the 3/2 mode $r_s \sim$ 26 cm, where as for the 2/1 mode $r_s \sim$ 36 cm. For an 8 cm 3/2 island the confinement is degraded by 8.3% according to the belt model. To obtain similar confinement degradation, the 3/2 NTM must not be present and the 2/1 mode must be suppressed to less than 3 cm wide. Note that the island widths calculated throughout this work use a large aspect ratio approximation [21], proportional to the square root of the poloidal field fluctuation amplitude ($\tilde{B}_\theta$) measured at the wall by a Mirnov probe, and a 2/3 correction measured using ECE.

Beyond fusion performance, stability to tearing mode locking [22] will ultimately limit the allowable 2/1 or 3/2 island size [23] for hybrid discharges. For ITER low q_{95} discharges, it has been estimated that 2/1 and 3/2 island full widths will be limited to less than 5 and 8 cm, respectively to avoid locking [24,25] and potentially causing a disruption.

In Fig. 3, a hybrid discharge with $q_{95} \sim 4.3$ is shown. Once the discharge reaches stationary plasma conditions, the neutral beam injected power is raised for a short period to rapidly increase

β_N and deliberately destabilize a 2/1 NTM. Once the tearing mode is generated, neutral beam heating is returned to the level applied prior to the creation of the mode. This is then followed by active suppression of the mode by applying ECCD from two gyrotrons focused at the 2/1 rational surface. At ~5700 ms the 2/1 mode amplitude is completely suppressed. Immediately after suppression, sawteeth appear for the first time in the discharge. This is a nearly identical finding as in the 3/2 suppressed case [9]. It must be noted that the q-profile was evolving downward during the ECCD suppression period. However, the sawteeth are not believed to be coincident with changes in the overall current profile, and instead result from the loss of the 2/1 mode.

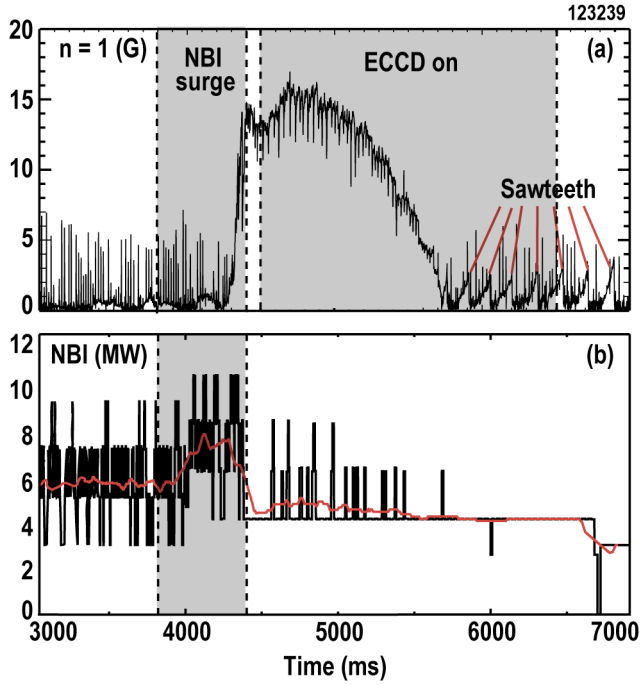

Fig. 3. (a) The amplitude of an n=1 tearing mode (G) followed by sawteeth after complete suppression, (b) total neutral beam injected power (MW).

Flux pumping is present during the partially suppressed period of the 2/1 NTM. Figure 4 shows flux pumping profiles taken from an ensemble average of 51 ELM-NTM coupling events. The data was taken over the 4500 to 5500 ms period of the discharge shown in Fig. 3, where ECCD is actively suppressing the mode but has not completely suppressed it. A clear inversion of the magnetic field strength, safety factor and externally driven current density profiles (including Ohmic) at the 2/1 rational surface can be seen. Also, there is a characteristic spike in the bootstrap current density at the 2/1 rational surface, which is consistent with an increase in the pressure gradient due to island shrinking. This J_{BS} is determined from a direct MSE measurement of the Pfirsch-Schlüter current density and the application of neoclassical theory in a simplifying limit [12]. Note, the smaller than expected increase in $q_{\min}$ and decrease in core J_{CD} indicate that the net plasma current increased at the ELM crash, which is unlikely. This can be partly explained by the fact that only changes due to ELMs are considered in this analysis and a correction for the overall evolution in the current profile was not applied.

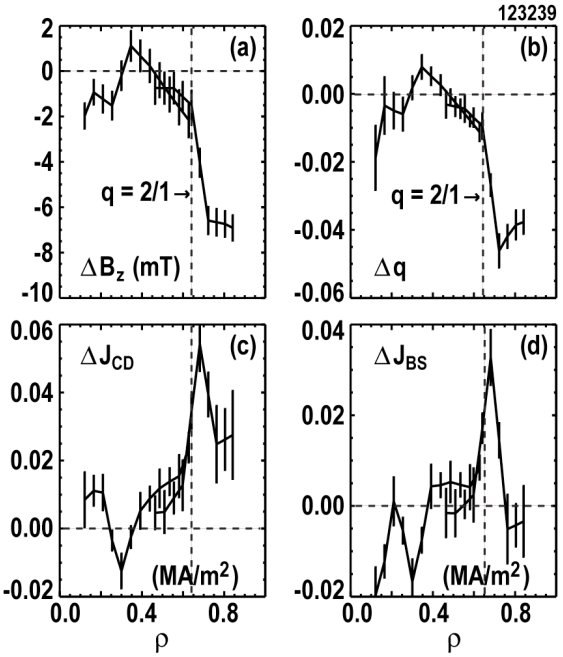

Fig. 4. Changes in radial profiles during ELM-NTM coupling events for (a) vertical magnetic field strength (mT), (b) safety factor, (c) externally driven current density (MA/m^2), and (d) bootstrap current density (MA/m^2). The profiles where determined from ensemble averaging MSE data over 51 ELM-NTM coupling events.

Previous work has shown 3/2-hybrid flux-pumping is strongest at higher β_N values [Ref. [10], Fig. 5]. Of the two discharges the lower β_N (lower flux-pumping) case had sawteeth. Further analysis of these discharges show that for the same average neutral beam power the smaller β_N case also has a 12% larger 3/2 island. This can be seen in Fig. 5. Recall [26] $w_{sat} \propto \beta_p L_q / L_p$, where w_{sat} is the saturated island width, L_p and L_q are the pressure gradient length and magnetic shear length, respectively. Therefore, a difference in the pressure or safety factor profile can result in a different saturated island width for the same beta. In discharge 123204, larger L_q and smaller L_p resulted in a larger island at smaller β_N. This suggests a favorable relationship exists between flux-pumping and a smaller island.

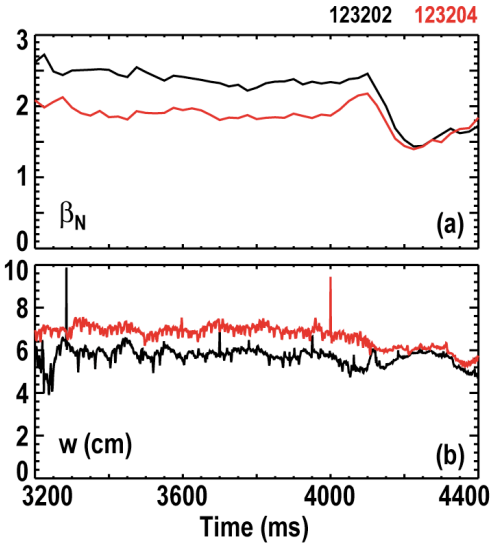

Fig. 5. For two discharges showing different 3/2 flux-pumping in Ref. [9]: (a) normalized beta (b) full island width (cm) measured by a Mirnov probe array.

To further elucidate hybrid flux-pumping, two parameters must be defined. The strength of the flux-pumping is taken as the total displacement of the safety factor across the rational surface (Δq_{tot}). This is found by taking the difference between the maximum and minimum values of the Δq-profiles. The distance between the NTM and the ELMing pedestal ($\Delta \rho_{ped}$) is defined as the difference between the normalized minor radius (ρ) at the rational surface and ρ at q_{95}. Table I compares the flux-pumping strength, proximity to the ELM region, normalized beta and island width for the discharges discussed.

Table I
Comparison of flux-pumping strength; the discharge number, tearing mode poloidal (m) and toroidal mode numbers (n), flux-pumping strength (Δq_{tot}), distance between the mode rational surface and q_{95} in terms of normalized poloidal flux ($\Delta \rho_{ped}$), normalized beta (β_N), and average island width (w).

Discharge	m/n	Δq_{tot}	$\Delta \rho_{ped}$	β_N	w (cm)
104268	2/1	0.10	0.36	2.5	8.5
123239	2/1	0.06	0.30	1.9	6.4
123202	3/2	0.06	0.51	2.7	5.8
123204	3/2	0.02	0.45	1.9	6.6

The flux-pumping strength is predominantly dependent on β_N and the proximity of the mode to the edge pedestal, and appears invariant with respect to the island size. For the same β_N and nearly the same island width (123204 and 123239) the mode closer to the pedestal (123239) shows a factor of three stronger flux-pumping than the larger distance case (123204). The two cases containing 2/1 modes (104268 and 123239) have roughly the same proximity to the pedestal, but the larger β_N case (104268) has the stronger flux-pumping. This β_N dependence is also true for the previously published [9] 3/2 mode discharges (123202 and 123204). The strongest overall flux-pumping (104268) occurs when both the proximity to the ELM and β_N are greatest. Likewise, the weakest flux-pumping (123204) occurs when both β_N is low and the island is furthest from the pedestal. While independent variation of the island width is required to draw any strong conclusions, there appears to be no clear connection between the size of the island and the strength of the flux-pumping. This suggests that the rational surfaces of the respective island chains are serving only as a radial surfaces around which poloidal flux is able to pivot. Partial suppression of the island chains should therefore not impede flux-pumping, rather the higher achievable β_N afforded from the improved energy confinement, should amplify it.

IV. ELM-NTM COUPLING

No explanation currently exists for how ELM-NTM coupling is connected to the rapid global redistribution of the current profile. Only a local spike in the bootstrap current density at the rational surface can be explained by an increased pressure gradient resulting from island shrinking. Despite this fact, it is still informative to consider the dynamics of this ELM-NTM coupling. This section describes the shrinkage and recovery phases of the NTM width as well as a connection found between ELM size and the degree of island shrinkage.

For this work, saturated 2/1 NTMs were considered. The radial proximity of 2/1 NTMs to the Mirnov probes produces the largest $\tilde{B}_\theta$ amplitudes, and hence results in the greatest signal-to-noise for studying mode width evolution. Electron cyclotron emission (ECE) radiometry [27] temperature ($\tilde{T}_e$) and MSE density [28,29] fluctuation ($\tilde{n}_e$) data are also considered and agree well with probe width measurements.

These multiple fluctuation diagnostics show drops in amplitude associated with the 2/1-ELM coupling. Figure 6 shows significant drops in the NTM $\tilde{n}_e$, $\tilde{T}_e$, and $\tilde{B}_\theta$ amplitudes during ELMs. Note, the Mirnov probe measurement is taken at the wall, the MSE channel is located in the edge pedestal on the low field side midplane, and the ECE channel is measuring near the mode rational surface on the high field side of the machine. Despite these very different radial locations each signal exhibits a similar drop in amplitude correlated with a filterscope measurement of the ELM-generated D_α light [30].

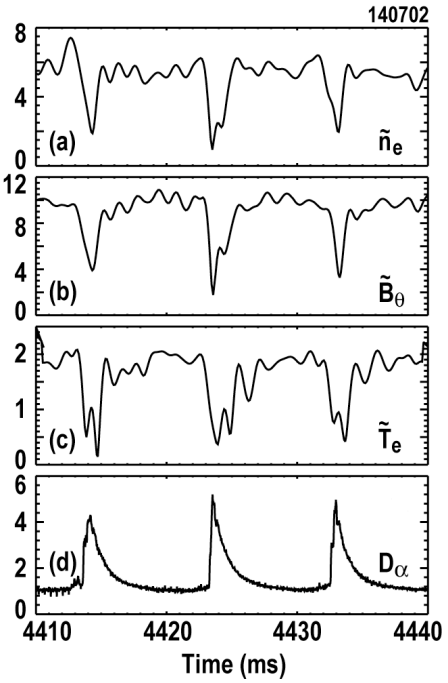

Fig. 6. Amplitudes of arbitrary units (a) electron density fluctuation $\tilde{n}_e$ within the pedestal (MSE) (b) poloidal field fluctuation $\tilde{B}_\theta$ at the wall (Mirnov probe) (c) high field side core electron temperature fluctuation $\tilde{T}_e$ near the rational surface (ECE) (d) filterscope measurement of D_α light intensity indicating ELM events.

To verify that these drops in signal amplitude are due to island shrinkage as opposed to global plasma displacements the entire 40 channel ECE array was used to estimate the island structure. Figure 7(a) shows the island structure ~ 600 μs before and after an ELM event measured on the high field side of the machine. This contour plot is detrended by removing the absolute value of the temperature for each channel and only considering the fluctuating component $\tilde{T}_e$. The blue and red colors represent temperatures less than and greater than the local absolute temperature, respectively. A clear 180° phase inversion occurs across the rational surface. The rational surface remains stationary across the ELM event. Figure 7(b) shows two normalized cross-cuts of the island O-point, before (1) and after the ELM (2). These fluctuation profiles are separately normalized on either side of the rational surface using the local maximum $\tilde{T}_e$ amplitude. The peak fluctuation amplitudes correspond to the maximum radii of the island separatrix. This means that the distance between the peak amplitudes in Fig. 7(b) provides an estimate of the full island width. The distance between the peaks in profile 1 is about 4 cm larger than that of profile 2, therefore the island shrinks by ~ 4 cm across the ELM. This particular ELM was relatively small at less than 20 kJ for a plasma with total stored energy of 750 kJ. For larger ELMs greater than 80 kJ the drop in island width would require a 15 cm radial displacement of the rational surface to explain the drop in $\tilde{B}_\theta$ measured at the wall, which is far greater than is believed physically possible.

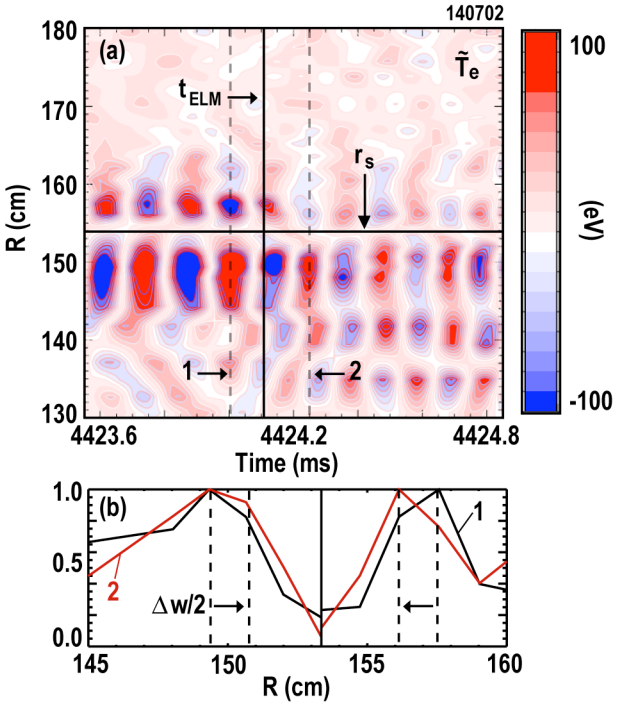

Fig. 7. Electron cyclotron radiometry measurements of poloidal island shrinking, (a) island structure, time of ELM crash (t_{ELM}), time before ELM (1) and time after ELM (2), (b) normalized cross cuts (1) and (2) of the island before the ELM (black-1) and after the ELM (red-2).

A. ISLAND SHRINKING AND ELM SIZE

ELM-NTM coupling can be considered in two distinct regions, a fast timescale drop in the island width followed by a resistive recovery to the original saturated island width. This section discusses a relationship between a drop in island width and the size of the ELM.

To isolate ELMs as the only MHD perturbing the island, the 2/1 modes were restricted to a saturated island size (between ELMs) of $\tilde{B}_\theta \sim 15$ G, and auxiliary power remained constant. This strict criterion on auxiliary heating allows β_N to be restricted to a narrow region between 1.4 and 1.6. To maintain a constant distance between the rational surface and the edge pedestal, q_{95} for most cases was held at 4. One shot had q_{95} of 5, but still showed the same general trend. The size and period of the perturbing ELMs were varied by changes to the plasma shape [31], resulting in minor radial differences between the edge pedestal and the rational surface.

The size of the ELM was determined from a diamagnetic loop measurement of the drop in the plasma internal stored energy (W). Diamagnetic loop measurements are only sensitive to coarse changes in W, therefore only relatively large ELMs (> 25 kJ) were considered. Due to an ELMs rapid change in W and the large skin time of the vacuum vessel wall, accurate measurements of the change in W require that the ELM period be longer than 50 ms. Note, this measurement may be an underestimate of the true ELM energy, since the recovery time of W is less than the diamagnetic measurement timescale. For the following comparison we are only interested in relative differences in ELM size and not the absolute change in energy due to an ELM. For consistency, infrared television (IRTV) measurements [32] of ELM divertor heat flux were compared with the diamagnetic loop measured W.

Figure 8 shows a clear upward trend between the fractional stored energy loss ($\Delta W/W$) of the ELM and the fractional drop in the island width ($\Delta w/w$). Each point plotted corresponds to a single ELM event. $\Delta W/W$ is calculated by subtracting the W measured after an ELM from W before the ELM and then dividing by the W before the ELM. An identical procedure is followed for calculating $\Delta w/w$. Note the good agreement between the IRTV measured ELM energy changes and the diamagnetic loop.

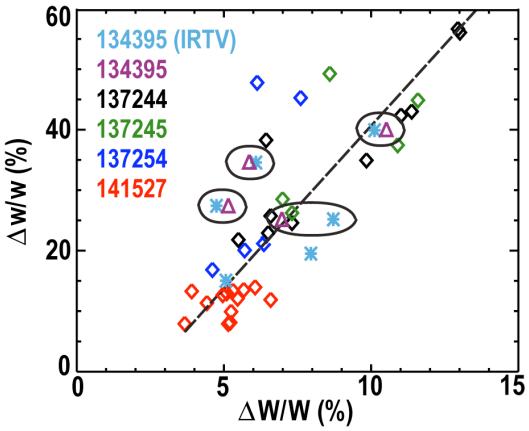

Fig. 8. Fractional drop in the magnetic island width (measured by Mirnov probes) vs. the fractional drop in stored energy associated with ELMs (measured by diamagnetic loop and IRTV divertor heat flux camera). Ovals indicate regions of good agreement between IRTV and diamagnetic loop measurements.

Proximity partly explains this stronger ELM-NTM coupling as the ELM size increases. ELM size is related to the radial depth of the most unstable mode [32]. Specifically, the dominant lower order mode numbers of the ELM are located deeper in the plasma and result in greater energy expulsion. Because of their greater depth, larger ELMs also have a greater proximity to core tearing modes improving their interaction. This finding parallels the result of the previous section where greater proximity of the tearing mode to the ELMing pedestal region caused greater flux-pumping. Here, instead of the rational surface being closer to the ELM, the ELM is closer to the tearing mode.

B. RESISTIVE RECOVERY OF THE ISLAND WIDTH

To develop a more complete understanding of ELM-NTM coupling requires examination of the slow recovery phase observed after an ELM. This section shows that the evolution of the island width following an ELM is fully described using a neoclassical description.

The simplest form of the modified Rutherford equation (MRE) [33] that contains neoclassical effects is taken as,

$$\frac{\tau_R}{r_s^2}\frac{dw}{dt} = \Delta' + \frac{\varepsilon^{1/2} L_q \beta_p}{L_p w} \quad ,$$

where $L_q = q/(dq/dr)$ and $L_p = -p/(dp/dr)$, τ_R is the time constant for resistive diffusion within the island region, r_s is the minor radius of the rational surface, ε is the local inverse aspect ratio at r_s, β_p is the ratio of kinetic pressure to poloidal magnetic pressure, and Δ' is the classical stability index. By applying an impulse perturbation to this form of the MRE and expanding, an accurate description of the ELM-NTM coupling resistive recovery phase is obtained. The relatively fast impulse at an ELM and the relatively long τ_R in the MRE, suggests an ideal coupling of the NTM to the ELM, which is a peeling/ballooning mode; this could result in a transient negative "pole" in the Δ' term [34]. The evolution of the island width w is taken as

$$w = w_{sat} - \delta_0 e^{-t/\tau_{relax}} \quad , \tag{2}$$

where w_{sat} is the saturated island width, δ_0 is the downward going impulse perturbation, t is time, and τ_{relax} is a time constant given by,

$$\tau_{relax} = \frac{w_{sat}^2 L_p \tau_R}{r_s^2 \varepsilon^{1/2} L_q \beta_p} \quad . \tag{3}$$

Figure 9 shows excellent agreement between the measured island width and the analytical description given by Eq. (2). The relaxation time constant for this discharge was calculated to be

11.3 ms. The drop (δ_0) is not analytically determined and was taken from the local minimum of the measured values for each of the coupling events.

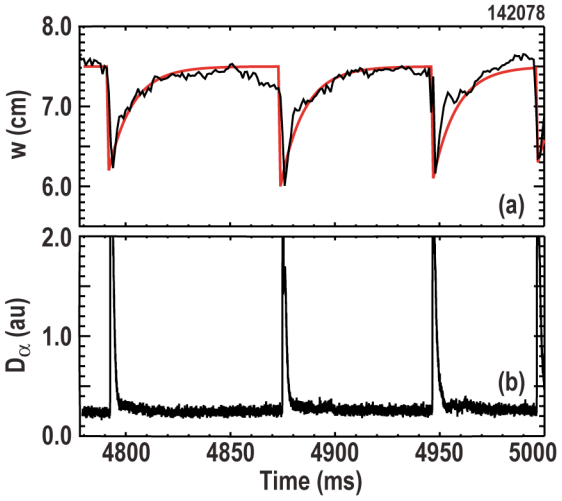

Fig. 9. For ELM-NTM coupling events, (a) Black – measured island widths. Red – analytical expression for the recovery given by Eq. (2). (b) Filterscope measurement of ELM induced D_α emissions.

V. CONCLUSIONS

ELM-NTM coupling induced magnetic flux-pumping has shown identical sawtooth avoidance in 2/1 hybrid-like stationary discharges as has been seen in 3/2 hybrids. For the complete active suppression of a 2/1 tearing mode sawteeth appear and persist throughout a discharge. The 2/1-flux-pumping is more than twice as strong as is observed in a typical 3/2 case, and clear characteristic changes in the radial profiles of B_z, q, J_{CD}, and J_{BS} are present during partial ECCD suppression. Achieving comparable energy confinement in the 2/1-hybrid will require partial suppression of the mode width, but the ultimate limit on the allowable island size will likely be defined by the avoidance of wall locking. The strength of flux-pumping and ELM-NTM coupling has a strong upward dependence on β_N and the proximity of the mode to the ELMing pedestal, and appears to be largely invariant with respect to the size of the island. The island seems to serve as a radial pivot surface around which poloidal flux is pumped from the core to the edge.

ELM-NTM coupling consists of an fast timescale drop in the island width followed by a resistive recovery. The drop in island width increases as the size of the ELM increases, and the recovery can be described analytically by applying a downward going impulse perturbation to the MRE.

These findings suggest that a 2/1 hybrid-like discharge may outperform existing 3/2 hybrids at lower q_{95}. Partial suppression of a 2/1 island should provide a dual effect of improving energy confinement while allowing intrinsically stronger 2/1 flux-pumping to sustain a flatter current profile without sawteeth. Furthermore, beta would no longer be limited by the onset of a 2/1 mode allowing values to reach the no-wall limit.

REFERENCES

[1] A. C. C. Sips, *et al.*, Plasma Phys. Control. Fusion **44**, B69 (2002).

[2] E. Joffrin, *et al.*, Plasma Phys. Control. Fusion **45**, A367 (2003).

[3] A. Isayama, Y. Kamada, N. Hayashi, T. Suzuki, T. Oikawa, T. Fujita, T. Fukuda, S. Ide, H. Takenaga, K. Ushigusa, T. Ozeki, Y. Ikeda, N. Umeda, H. Yamada, M. Isobe, Y. Narushima, K. Ikeda, S. Sakakibara, and K. Yamazaki, Nucl. Fusion **43**, 1272 (2003).

[4] T. C. Luce, *et al.*, Nucl. Fusion **41**, 1585 (2001).

[5] T. C. Luce, M. R. Wade, J. R. Ferron, P. A. Politzer, A. W. Hyatt, A. C. C. Sips, M. Murakami, Phys. Plasmas **11**, 2627 (2004).

[6] J. L. Luxon, Nucl. Fusion **42**, 614 (2002).

[7] P. N. Yushmanov, T. Takizuka, K. S. Riedel, O. J. W. F. Kardaun, J. G. Cordey, S. M. Kaye, and D. E. Post, Nucl. Fusion **30**, 1999 (1990).

[8] R. J. Buttery, R. J. La Haye, P. Gohil, G. L. Jackson, H. Reimerdes, E. J. Strait, and the DIII-D Team, Phys. Plasmas **15**, 056115 (2008).

[9] M. R. Wade, T. C. Luce, R. J. Jayakumar, P. A. Politzer, A. W. Hyatt, J. R. Ferron, C. M. Greenfield, M. Murakami, C. C. Petty, R. Prater, J. C. DeBoo, R. J. La Haye, P. Gohil, and T. L. Rhodes, Nucl. Fusion **45**, 407–416 (2005).

[10] C. C. Petty, M. E. Austin, C. T. Holcomb, R. J. Jayakumar, R. J. La Haye, T. C. Luce, M. A. Makowski, P. A. Politzer, and M. R. Wade, Phys. Rev. Lett. **102**, 045005 (2009).

[11] F. M. Levington, R. J. Fonck, G. M. Gammel, R. Kaita, H. W. Kugel, E. T. Powell, and D. W. Roberts, Phys. Rev. Lett. **63**, 2060 (1989).

[12] D. Wroblewski, and L. L. Lao, Rev. Sci. Instrum. **63**, 5140 (1992).

[13] C. C. Petty, P. A. Politzer, and Y. R. Lin-Liu, Plasma Phys. Controlled Fusion **47**, 1077 (2005).

[14] M. Maraschek, G. Gantenbein, Q. Yu, H. Zohm, S. Gunter, F. Leuterer, and A. Manini, Phys. Rev. Lett. **98**, 025005(2007).

[15] A. Isayama, G. Matsunaga, T. Kobayashi, S. Moriyama, N. Oyama, Y. Sakamoto, T. Suzuki, H. Urano, N. Hayashi, Y. Kamada, T. Ozeki, Y. Hirano, L. Urso, H. Zohm, M. Maraschek, J. Hobirk, and K. Nagasaki, Nucl. Fusion **49**, 055006 (2009).

[16] R. J. La Haye, S. Günter, D. A. Humphreys, J. Lohr, T. C. Luce, M. E. Maraschek, C. C. Petty, R. Prater, J. T. Scoville, and E. J. Strait, Phys. Plasmas **9**, 2051 (2002).

[17] D. A. Humphreys, J. R. Ferron, R. J. La Haye, T. C. Luce, C. C. Petty, R. Prater, and A. S. Welander, Phys. Plasmas **13**, 056113 (2006).

[18] C. C. Petty, R. J. La Haye, T. C. Luce, D. A. Humphreys, A. W. Hyatt, J. Lohr, R. Prater, E. J. Strait, and M. R. Wade, Nucl. Fusion **44**, 243 (2004).

[19] R. Prater, R. J. La Haye, T. C. Luce, C. C. Petty, E. J. Strait, J. R. Ferron, D. A. Humphreys, A. Isayama, J. Lohr, K. Nagasaki, P. A. Politzer, M. R. Wade, and A. S. Welander, Nucl. Fusion **47**, 371 (2007).

[20] P. A. Politzer, C. C. Petty, R. J. Jayakumar, T. C. Luce, M. R. Wade, J. C. DeBoo, J. R. Ferron, P. Gohil, C. T. Holcomb, A. W. Hyatt, J. Kinsey, R. J. La Haye, M. A. Makowski, and T. W. Petrie, Nucl. Fusion **48**, 075001 (2008).

[21] R. J. La Haye, R. J. Buttery, S. Guenter, G. T. A. Huysmans, M. Maraschek, and H. R. Wilson, Phys. Plasmas **7**, 3349 (2000).

[22] J. T. Scoville, R. J. La Haye, A. G. Kellman, T. H. Osborne, R. D. Stambaugh, E. J. Strait, and T. S. Taylor, Nucl. Fusion **31**, 875 (1991).

[23] F. A. G. Volpe, M. E. Austin, R. J. La Haye, J. Lohr, R. Prater, E. J. Strait, and A. S. Welander, Phys. Plasmas **16**, 102502 (2009).

[24] R. J. La Haye, R. Prater, R. J. Buttery, N. Hayashi, A. Isayama, M. E. Maraschek, L. Urso, and H. Zohm, Nucl. Fusion **46**, 451 (2006).

[25] R. J. La Haye, J. R. Ferron, D. A. Humphreys, T. C. Luce, C. C. Petty, R. Prater, E. J. Strait, and A. S. Welander, Nucl. Fusion **48**, 054004 (2008).

[26] Z. Chang, J. D. Callen, E. D. Fredrickson, R. V. Budny, C. C. Hegna, K. M. McGuire, and M. C. Zarnstorff, Phys. Rev. Lett. **74**, 4663 (1995).

[27] M. E. Austin and J. Lohr, Rev. Sci. Instrum. **74**, 1457 (2003).

[28] T. Suzuki, T. Fujita, N. Oyama, A. Isayama, G. Matsunaga, T. Oikawa, N. Asakura, and M. Takechi, Rev. Sci. Instrum. **77**, 10E914 (2006).

[29] J. D. King, M. A. Makowski, C. T. Holcomb, S. L. Allen, D. N. Hill, R. J. La Haye, F. Turco, C. C. Petty, M. A. Van Zeeland, T. L. Rhodes, W. H. Meyer, R. Geer, and E. C. Morse, Rev. Sci. Instrum. **82**, 033515 (2011).

[30] R. J. Colchin, D. L. Hills, R. Maingi, C. C. Klepper, and N. H. Brooks, Rev. Sci. Instrum. **74**, 2068 (2003).

[31] P. B. Snyder, H. R. Wilson, J. R. Ferron, L. L. Lao, A. W. Leonard, T. H. Osborne, A. D. Turnbull, D. Mossessian, M. Murakami, X. Q. Xu, Phys. Plasmas **9**, 2037 (2002).

[32] D. N. Hill, T. Petrie, M. Ali Mahdavi, L. Lao and W. Howl, Nucl. Fusion **28**, 902 (1988).

[33] R. J. La Haye, Phys. Plasmas **13**, 055501 (2006).

[34] D. P. Brennan, A. D. Turnbull, M. S. Chu, R. J. La Haye, L. L. Lao, T. H. Osborne, and S. A. Galkin, Phys. Plasmas **14**, 056108 (2007).

ACKNOWLEDGMENT

This work was performed under the auspices of the U.S. Department of Energy by Lawrence Livermore National Laboratory under USDOE Grant No. DE-AC52-07NA27344 and in part by the U.S. Department of Energy under DE-FG03-89ER51116, DE-FC02-04ER54698, DE-FG02-92ER54139 and DE-FG03-97ER54415.

P.O. BOX 85608 SAN DIEGO, CA 92186-5608 (858) 455-3000